International Journal of Dynamics and Control (2023) 11:2179–2192
https://doi.org/10.1007/s40435-023-01134-4

A generalized Caputo-type fractional-order neuron model under the electromagnetic field

Pushpendra Kumar[1] · **Vedat Suat Erturk**[2] · **Swati Tyagi**[3] · **Jozef Banas**[4] · **A. Manickam**[5]

Received: 13 October 2022 / Revised: 1 January 2023 / Accepted: 1 February 2023 / Published online: 2 March 2023

Abstract
This article considers a fractional-order neuron model under an electromagnetic field in terms of generalized Caputo fractional derivatives. The motivation for incorporating fractional derivatives in the previously proposed integer-order neuron model is that the fractional-order model impresses with efficient effects of the memory, and parameters with fractional orders can increase the model performance by amplifying a degree of freedom. The results on the uniqueness of the solution for the proposed neuron model are established using well-known theorems. The given model is numerically solved by using a generalized version of the Euler method with stability and error analysis. Several graphical simulations are performed to capture the variations in the membrane potential considering no electromagnetic field effects, various frequency brands of external forcing current, and the amplitude and frequency of the external magnetic radiation. The impacts of fractional-order cases are clearly justified.

Keywords Neuron model · Electromagnetic induction · Generalized Caputo fractional derivative · Euler method · Error estimation · Stability

✉ Pushpendra Kumar
kumarsaraswatpk@gmail.com; pkkumar@uj.ac.za

Vedat Suat Erturk
vserturk@omu.edu.tr

Swati Tyagi
styagi99@gmail.com

Jozef Banas
jbanas@prz.edu.pl

A. Manickam
manickammaths2011@gmail.com

1 Institute for the Future of Knowledge, University of Johannesburg, PO Box 524, Auckland Park 2006, South Africa

2 Department of Mathematics, Faculty of Arts and Sciences, Ondokuz Mayis University, 55200 Atakum, Samsun, Turkey

3 Department of Mathematics, Amity University Punjab, Mohali, Punjab 140306, India

4 Department of Nonlinear Analysis, Rzeszow University of Technology, al. Powstancow Warszawy 8, 35-959 Rzeszow, Poland

5 Department of Mathematics, School of Advanced Sciences and Languages, VIT Bhopal University, Bhopal-Indore Highway, Kothrikalan, Sehore, Madhya Pradesh 466114, India

1 Introduction

Heinrich Wilhelm Gottfried von Waldeyer-Hartz, a German scientist, is credited with coining the term "neuron" in 1891. Neurons are nerve cells that send and receive messages from the brain. The neuron is made up of a cell body, or soma, with branching dendrites that act as signal receivers and an axon that carries nerve signals. The axon terminals send the electrochemical signal across a synapse at the opposite end of the axon (the space between the axon terminal and the receiving cell).

Neuron dynamics have been described using a variety of models. A set of first-order ordinary differential equations has been used to describe the dynamic behavior that a neuron model exhibits. The Hodgkin–Huxley (HH) model [1], which takes into account the ionic process and current on the surface of the cell membrane, is the most well-known dynamical model of the biological neuron. It represents the behavior of the membrane action potential of the giant squid axon. The authors of [2] proposed the Leaky Integrate and Fire neuron (LIF), which is generally used in experiments on large networks. In [3], a silicon hardware implementation of neurons considered in neuromorphic circuits was explored. The accuracy of the LIF neuron was not good because of its

unrealistic simplicity, so it did not match with experimental outputs. In ref. [4], an optimized realization of the Morris-Lecar neuromorphic model was introduced. In ref. [5], the Hindmarsh–Rose neuron model was considered to take memristors to imitate the connection between the magnetic flux and membrane potential of the electromagnetic field. Several neuron models [6–8] have been introduced to analyze the electrical behaviors of neuron and the outcomes are used to produce similar phases and modes such as spiking, quiescent, bursting, and even chaotic states.

Fractional calculus, one of the most useful areas of research in applied mathematics, contains various types of differential and integral operators [9–12]. Fractional-order operators have been successfully implemented to describe a number of real-world problems. The authors in [13] introduced a fractional mathematical model for the huanglongbing transmission within a citrus tree. In [14], a study on the structure of the alkali-silica chemical reaction model using the Caputo fractional derivatives has been proposed. A Caputo-type corneal shape mathematical model with novel observations has been given in [15]. In [16], the optimal controls on the transmission of the bovine schistosomiasis epidemic model have been derived using fractional derivatives. The authors in [17] have introduced a fractal-fractional model of the AH1N1/09 virus. In [18], some novel analyses of a non-autonomous cardiac conduction model have been performed. In [19], the dynamics of a linear triatomic molecule have been defined using fractional derivatives.

The fractional derivatives have been implemented to analyze the models of neuron. In [20], the authors have proposed a fractional model with synchronization of electrically coupled neuron systems. In [21], a fractional leaky integrate and fire model has been given, considering neuronal spike timing adaptation. In [22], the fractional Izhikevich and Fitzhugh–Nagumo neuron modeling was introduced. In [23], the spiking and bursting behaviors of the fractional Izhikevich model were discussed. In [24], the authors have discussed low-voltage low-power integrable CMOS circuit application of integer- and fractional-order Fitzhugh–Nagumo neuron model. In [25], the structure of a neuron considering integer- and fractional-order discontinuous external magnetic flux has been given. In [26], a study on the fractional Izhikevich neuron model with synchronization and FPGA realization has been given. In [27], the authors proposed the synchronization of the fractional neuron model considering noise. In [28], an FPGA realization of a fractional-order neuron was discussed. In [29], the chimera state in the network of fractional Fitzhugh–Nagumo neurons has been investigated. In [30], a survey on the dynamics and implementation methods of fractional neuron models has been given. In [31], some novel analyses of the numerical approximations of fractional spiking neuron models have been given. In [32], a fractional-order Fitzhugh–Nagumo neuron model has been analyzed.

In this study, we propose a fractional-order neuron model, revising the previously published integer-order model [33] using the following generalized Caputo fractional derivative:

Definition 1 [34] The generalized Caputo-type fractional derivative, $D_{d_+}^{\gamma,\rho}$, of order $\gamma > 0$ is defined by

$$(D_{d_+}^{\gamma,\rho}u)(t) = \frac{\rho^{\gamma-n+1}}{\Gamma(n-\gamma)} \int_d^t s^{\rho-1}(t^\rho - s^\rho)^{n-\gamma-1}\left(s^{1-\rho}\frac{\mathrm{d}}{\mathrm{d}s}\right)^n u(s)\mathrm{d}s, \quad t > d, \quad (1)$$

where $\rho > 0, d \geq 0,$ *and* $n-1 < \gamma \leq n$.

We apply fractional derivatives because the fractional-order model contains memory in the system, and the parameters with fractional order can enrich the model performance, providing one degree of freedom. The paper is organized in the following sections: In Sect. 2, the description of the proposed fractional-order model is given with the results of the existence of a unique solution. In Sect. 3, the numerical solution of the proposed model is derived using a modified version of the Euler method along with the stability and error estimation of the scheme. In Sect. 4, the graphical simulations are given. In Sect. 5, the results are concluded.

2 Model description

The proposed revised form of an integer-order neuron model [33] using the generalized Caputo fractional derivative is given by

$$\begin{aligned}
{}_0^C D_t^{\gamma,\rho} v &= -\left(\frac{v^3}{3} - k_1 v\right) - i + I_{ext} + \lambda_H(\alpha + 3\beta w^2)v,\\
{}_0^C D_t^{\gamma,\rho} i &= v - k_2 i - \lambda_E(a + bq^2)i,\\
{}_0^C D_t^{\gamma,\rho} q &= k_3 i,\\
{}_0^C D_t^{\gamma,\rho} w &= -k_4 v,
\end{aligned} \quad (2)$$

where $I_{ext} = I_1 \sin(\pi f_1 t) + I_2 \cos(\pi f_2 t)$ defines external forcing current with different frequencies f_1, f_2 and currents I_1, I_2. ${}_0^C D_t^{\gamma,\rho}$ denotes the generalized Caputo derivative with order γ along with extra parameter ρ. Moreover v, i, q, and w define the voltage, current, charge, and magnetic flux in the case of dimensionless parameters, respectively. λ_H and λ_E are the switching factors of the magnetic and electric field. Other parameters are k_1, k_2, k_3, k_4 and α, β, a, b are described briefly in ref. [33]. The reason for showing an interest in the given model is the proposed model contains multiple factors, namely, electromagnetic field effects, various frequency brands of external forcing current, and the amplitude and frequency of the external magnetic radiation,

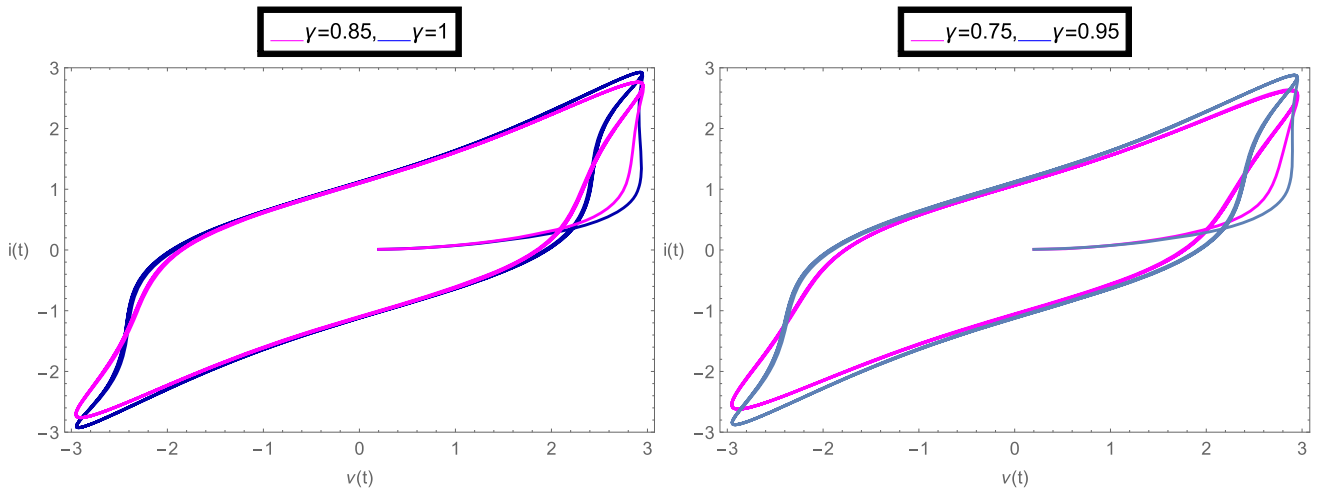

(a) $v(t)$ vs $i(t)$ (b) $v(t)$ vs $i(t)$

Fig. 1 Parameter values: $k_1 = 1.0$, $I_1 = 6.0$, $f_1 = 0.06$, $I_2 = 6.0$, $f_2 = 0.06$, $\lambda_H = 0.0$, $\alpha = 1.0$, $\beta = 0.02$, $k_2 = 1.0$, $\lambda_E = 0.0$, $a = 0.2$, $b = 0.1$, $k_3 = 1.0$, $k_4 = 0.01$

to capture the variations in the membrane potential. Also, incorporating an extra parameter ρ along with fractional-order γ adding one more degree of freedom, makes the proposed methodology advanced to the general Caputo case.

For further investigations, let us define

$$\begin{cases} x_1(t,v,i,q,w) = -\left(\frac{v^3}{3} - k_1 v\right) - i \\ \qquad\qquad +I_{ext} + \lambda_H(\alpha + 3\beta w^2)v, \\ x_2(t,v,i,q,w) = v - k_2 i - \lambda_E(a + bq^2)i, \\ x_3(t,v,i,q,w) = k_3 i, \\ x_4(t,v,i,q,w) = -k_4 v. \end{cases} \tag{3}$$

and

$$u(t) = \begin{cases} v(t) \\ i(t) \\ q(t) \\ w(t) \end{cases}, \quad u_0(t) = \begin{cases} v_0(t) \\ i_0(t) \\ q_0(t) \\ w_0(t) \end{cases},$$

$$x(t,u(t)) = \begin{cases} x_1(t,v,i,q,w) \\ x_2(t,v,i,q,w) \\ x_3(t,v,i,q,w) \\ x_4(t,v,i,q,w) \end{cases}. \tag{4}$$

Then, the proposed model (2) can be expressed in terms of the following initial value problem (IVP) for the given function $u(t)$ with singular kernel $x(t,u)$ on the time interval $[0,T]$:

$${}^{C}_{0}D^{\gamma,\rho}_{t} u(t) = x(t,u(t)),\ t \in [0,T],\ 0 < \gamma \le 1, \tag{5a}$$

$$u(0) = u_0, \tag{5b}$$

The related Volterra integral equation (VIE) of the IVP (5a)–(5b) is given by [34]

$$u(t) = u(0) + \frac{\rho^{1-\gamma}}{\Gamma(\gamma)} \int_0^t s^{\rho-1}(t^\rho - s^\rho)^{\gamma-1} x(s,u)\mathrm{d}s. \tag{6}$$

Firstly, we recall the results regarding the existence of unique solution for the above given IVP (5a) and (5b) using following theorems.

Theorem 1 (Existence) [35]. *For* $0 < \gamma \le 1$, $u_0 \in \mathbb{R}$, $T^* > 0$, $J > 0$, *consider the set* $\zeta := \{(t,u) : t \in [0,T^*],\ |u - u_0| \le J\}$ *and define the continuous function* $x : \zeta \to \mathbb{R}$. *Let* $M := \sup_{(t,u)\in\zeta} |x(t,u)|$ *and*

$$T = \begin{cases} T^*, & if\, M = 0, \\ min\{T^*, \left(\frac{J\Gamma(\gamma+1)\rho^\gamma}{M}\right)^{\frac{1}{\gamma}}\} & otherwise. \end{cases} \tag{7}$$

Then, a function $u \in \mathcal{C}[0,T]$ *exists and it satisfies the IVP* (5a) *and* (5b).

Theorem 2 (Uniqueness) [35]. *Let* $u(0) \in \mathbb{R}$, $J > 0$, $T^* > 0$, *and the set* ζ *given in Theorem* 1. *Consider the continuous function* $x : \zeta \to \mathbb{R}$ *satisfying the Lipschitz condition for variable u, i.e.,*

$$|x(t,u_1) - x(t,u_2)| \le V|u_1 - u_2|,$$

where $V > 0$ *is a constant independent to* $t, u_1,$ *and* u_2. *Then a unique solution* $u \in \mathcal{C}[0,T]$ *for the IVP* (5a) *and* (5b) *exists.*

Theorem 3 *The solution of model* (2) *is uniformly stable on* $[0,T]$ *for some* $T > 0$.

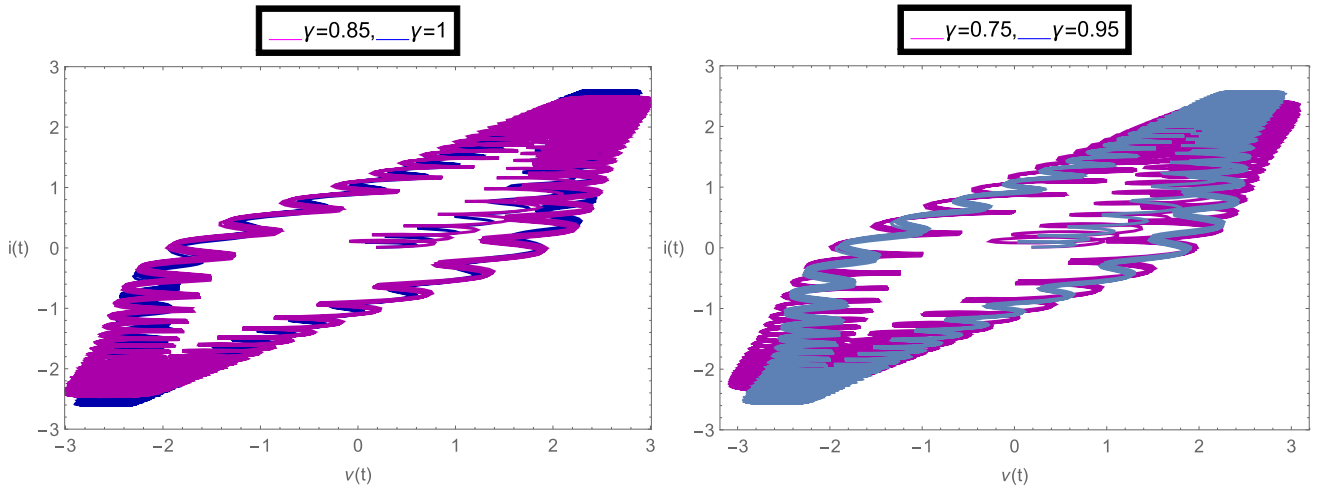

(a) $v(t)$ vs $i(t)$ (b) $v(t)$ vs $i(t)$

Fig. 2 Parameter values: $k_1 = 1.0$, $I_1 = 6.0$, $f_1 = 0.06$, $I_2 = 6.0$, $f_2 = 6.66$, $\lambda_H = 0.0$, $\alpha = 1.0$, $\beta = 0.02$, $k_2 = 1.0$, $\lambda_E = 0.0$, $a = 0.2$, $b = 0.1$, $k_3 = 1.0$, $k_4 = 0.01$

Proof On the contrary, we assume that there exists two solutions $u(t)$ and $v(t)$ of model (2) with initial conditions $u(0)$ and $v(0)$, such that

$$u(t) = u(0) + \frac{\rho^{1-\gamma}}{\Gamma(\gamma)} \int_0^t s^{\rho-1} (t^\rho - s^\rho)^{\gamma-1} x(s,u)\mathrm{d}s \tag{8}$$

$$v(t) = v(0) + \frac{\rho^{1-\gamma}}{\Gamma(\gamma)} \int_0^t s^{\rho-1} (t^\rho - s^\rho)^{\gamma-1} y(s,v)\mathrm{d}s \tag{9}$$

It follows that

$$\begin{aligned} \|u - v\| &\le \sup_t \left(\frac{\rho^{1-\gamma}}{\Gamma(\gamma)} \int_0^t s^{\rho-1} \left(t^\rho - s^\rho\right)^{\gamma-1} |x(s,u) \right. \\ &\quad \left. - y(s,v)|\mathrm{d}s \right) \\ &\le \sup_t \left(\frac{\rho^{1-\gamma}}{\Gamma(\gamma)} \int_0^t s^{\rho-1} \left(t^\rho - s^\rho\right)^{\gamma-1} \mathrm{d}s \right) \|x - y\| \\ &\le \frac{1}{\rho^\gamma \Gamma(\gamma+1)} h^\gamma \|x - y\|, \end{aligned} \tag{10}$$

where $h = \sup_t t^\rho$. We choose $\|x - y\| < \frac{\rho^\gamma \Gamma(\gamma+1)}{h^\gamma}\epsilon$. Then from (10), we conclude that

$$\|u - v\| < \epsilon.$$

This implies that the solution of model (2) is uniformly stable on $[0, T]$. □

3 Numerical solution using generalized Euler method

Several numerical methods have been derived to solve fractional-order systems in the last few years. In [36], a finite-difference predictor–corrector scheme was introduced for fractional differential equations. In [37], the authors have derived a short and efficient method to solve generalized Caputo-type differential equations. In [38], a modified predictor–corrector method has been introduced to solve generalized Caputo-type differential equations with delay. In [39], the authors have derived the generalized differential transform method to simulate impulsive fractional differential equations. In [40], the authors proposed a generalized Lucas polynomial sequence approach for fractional differential equations. In [41], a novel operation matrix scheme for solving generalized Caputo-type fractal–fractional differential equations has been derived. The author in [42] proposed an orthonormal ultraspherical operational matrix algorithm for generalized Caputo-type fractal–fractional Riccati equation.

In this section, we use the generalized Euler method given in [43] and using a non-uniform grid, to numerically solve the proposed IVP (5a) and (5b) (or model (2)). The time range $[a, T]$ is taken as a discrete set of points

$$\begin{cases} t_0 = a, \\ t_{j+1} = (t_j^\rho + h)^{1/\rho}, \quad j = 0, 1, \ldots, N-1, \end{cases} \tag{11}$$

where $h = \dfrac{T^\rho - t_0^\rho}{N}$. The solution is derived as approximations using a sequence u_j, $j = 0, 1, \ldots, N$, such that $u_k \approx u(t_k)(k = 1, 2, \ldots, j)$. The following Volterra integral equation can represent the exact solution of the given IVP:

$$u(t) = u(t_0) + \frac{\rho^{1-\gamma}}{\Gamma(\gamma)} \int_{t_0}^t s^{\rho-1} (t^\rho - s^\rho)^{\gamma-1} x(s,u)\mathrm{d}s. \tag{12}$$

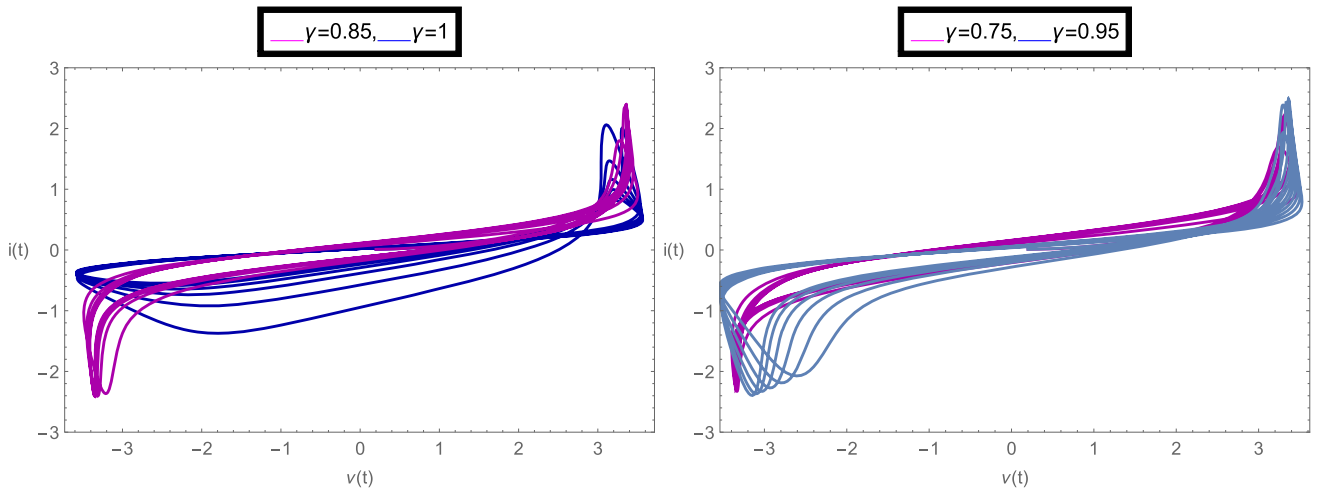

(a) $v(t)$ vs $i(t)$ (b) $v(t)$ vs $i(t)$

Fig. 3 Parameter values: $k_1 = 1.0$, $I_1 = 6.0$, $f_1 = 0.06$, $I_2 = 6.0$, $f_2 = 0.06$, $\lambda_H = 1.0$, $\alpha = 1.0$, $\beta = 0.02$, $k_2 = 1.0$, $\lambda_E = 1.0$, $a = 0.2$, $b = 0.1$, $k_3 = 1.0$, $k_4 = 0.01$

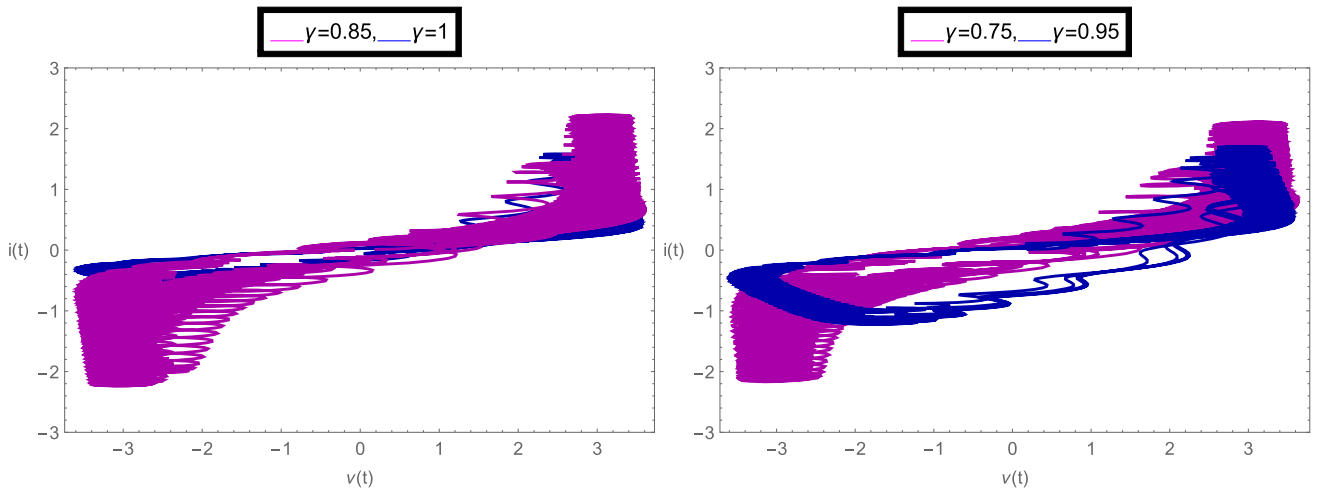

(a) $v(t)$ vs $i(t)$ (b) $v(t)$ vs $i(t)$

Fig. 4 Parameter values: $k_1 = 1.0$, $I_1 = 6.0$, $f_1 = 0.06$, $I_2 = 6.0$, $f_2 = 6.66$, $\lambda_H = 1.0$, $\alpha = 1.0$, $\beta = 0.02$, $k_2 = 1.0$, $\lambda_E = 1.0$, $a = 0.2$, $b = 0.1$, $k_3 = 1.0$, $k_4 = 0.01$

As a consequences, we can write

$$u(t_{j+1}) = u(t_0) + \frac{\rho^{1-\gamma}}{\Gamma(\gamma)} \sum_{k=0}^{j} \int_{t_k^\rho}^{t_{k+1}^\rho} s^{\rho-1}(t_{j+1}^\rho - s^\rho)^{\gamma-1} x(s, u(s)) \mathrm{d}s. \tag{13}$$

Taking $z = s^\rho$, we get

$$u(t_{j+1}) = u(t_0) + \frac{\rho^{-\gamma}}{\Gamma(\gamma)} \sum_{k=0}^{j} \int_{t_k^\rho}^{t_{k+1}^\rho} (t_{j+1}^\rho - z)^{\gamma-1} x(z^{1/\rho}, u(z^{1/\rho})) \mathrm{d}z. \tag{14}$$

In each of the subintervals, using composite rectangle rule, we define the approximation

$$\begin{aligned}
&\frac{\rho^{-\gamma}}{\Gamma(\gamma)} \sum_{k=0}^{j} \int_{t_k^\rho}^{t_{k+1}^\rho} (t_{j+1}^\rho - z)^{\gamma-1} x(t_k, u(t_k)) \mathrm{d}z \\
&= \frac{\rho^{-\gamma}}{\Gamma(\gamma)} \sum_{k=0}^{j} x(t_k, u(t_k)) \int_{t_k^\rho}^{t_{k+1}^\rho} (t_{j+1}^\rho - z)^{\gamma-1} \mathrm{d}z \\
&= \frac{\rho^{-\gamma}}{\Gamma(\gamma)} \sum_{k=0}^{j} x(t_k, u(t_k)) \left[\frac{-1}{\gamma} (t_{j+1}^\rho - z)^\gamma \Big|_{t_k^\rho}^{t_{k+1}^\rho} \right] \\
&= \frac{\rho^{-\gamma}}{\Gamma(\gamma+1)} \sum_{k=0}^{j} x(t_k, u(t_k)) \left[(t_{j+1}^\rho - t_k^\rho)^\gamma - (t_{j+1}^\rho - t_{k+1}^\rho)^\gamma \right].
\end{aligned} \tag{15}$$

The above approximation (15) gives the following explicit formula

$$u_{k+1} = u_0 + \frac{\rho^{-\gamma} h^{\gamma}}{\Gamma(\gamma+1)} \sum_{j=0}^{k} b_{j,k+1} x(t_j, u_j), \tag{16}$$

where

$$b_{j,k+1} = (k+1-j)^{\gamma} - (k-j)^{\gamma}. \tag{17}$$

Therefore, the algorithm of the numerical solution of the proposed system (2) is derived as follows:

$$\begin{aligned}
v_{k+1} &= v_0 + \frac{\rho^{-\gamma} h^{\gamma}}{\Gamma(\gamma+1)} \sum_{j=0}^{k} b_{j,k+1} \Big[-\left(\frac{v_j^3}{3} - k_1 v_j\right) \\
&\quad - i_j + I_{ext} + \lambda_H(\alpha + 3\beta w_j^2) v_j \Big], \\
i_{k+1} &= i_0 + \frac{\rho^{-\gamma} h^{\gamma}}{\Gamma(\gamma+1)} \sum_{j=0}^{k} b_{j,k+1} \big[v_j - k_2 i_j \\
&\quad - \lambda_E(a + b q_j^2) i_j \big], \\
q_{k+1} &= q_0 + \frac{\rho^{-\gamma} h^{\gamma}}{\Gamma(\gamma+1)} \sum_{j=0}^{k} b_{j,k+1} \big[k_3 i_j \big], \\
w_{k+1} &= w_0 + \frac{\rho^{-\gamma} h^{\gamma}}{\Gamma(\gamma+1)} \sum_{j=0}^{k} b_{j,k+1} \big[-k_4 v_j \big].
\end{aligned} \tag{18}$$

3.1 Stability analysis

Lemma 1 [44] *If $0 < \beta < 1$ and b is a nonnegative integer, then there exist two positive quantities $\mathcal{C}_{\beta,1}$ and $\mathcal{C}_{\beta,2}$ which depend on β, such that*

$$(b+1)^{\beta} - b^{\beta} \le \mathcal{C}_{\beta,1} (b+1)^{\beta-1},$$

and

$$(b+2)^{\beta+1} - 2(b+1)^{\beta+1} + b^{\beta+1} \le \mathcal{C}_{\beta,2} (b+1)^{\beta-1}.$$

Lemma 2 [44] *Let $d_{p,s} = (s-p)^{\beta-1} (p = 1, 2, \ldots, s-1)$ and $d_{p,s} = 0$ for $p \ge s, rh \le T, \beta, h, M, T > 0$ and r is a positive integer. Also, let $\sum_{p=r}^{p=s} d_{p,s} |e_p| = 0$ for $b > s \ge 1$. If*

$$|e_s| \le M h^{\beta} \sum_{p=1}^{s-1} d_{p,s} |e_p| + |\gamma_0|, \quad s = 1, 2, \ldots, r,$$

then

$$|e_r| \le \mathcal{C} |\gamma_0|, \quad r = 1, 2, \ldots$$

where $\mathcal{C}$ is a positive constant independent to h and r.

Theorem 4 *Let the kernel $x(t,u)$ satisfy the Lipschitz condition and u_m $(m = 1, \ldots, k+1)$ be the solution of Eqn. (16). Then, the proposed numerical method is conditionally stable.*

Proof Let $\tilde{u_0}$, and $\tilde{u_m}$ $(m = 0, \ldots, k+1)$ are the perturbations of u_0, and u_m, simultaneously. Then, the following approximation expression is obtained from Eq. (16)

$$\begin{aligned}
u_{k+1} + \tilde{u}_{k+1} &= u_0 + \tilde{u_0} + \frac{\rho^{-\gamma} h^{\gamma}}{\Gamma(\gamma+1)} \\
&\quad \sum_{k=0}^{j} b_{k,j+1} x(t_k, u_k + \tilde{u_k}),
\end{aligned} \tag{19}$$

where $b_{k,j+1} = [(j+1-k)^{\gamma} - (j-k)^{\gamma}]$.
Combining Eqs. (16) and (19), we obtain

$$\begin{aligned}
|\tilde{u}_{k+1}| &= |\tilde{u_0} + \frac{\rho^{-\gamma} h^{\gamma}}{\Gamma(\gamma+1)} \sum_{k=0}^{j} b_{k,j+1} (x(t_k, u_k + \tilde{u_k}) \\
&\quad - x(t_k, u_k))|.
\end{aligned} \tag{20}$$

From the triangle inequality and Lipschitz condition, we have

$$|\tilde{u}_{k+1}| \le \zeta_0 + \frac{\rho^{-\gamma} h^{\gamma} m_1 \mathcal{C}_{\gamma}}{\Gamma(\gamma+2)} \left(\sum_{k=1}^{j} b_{k,j+1} |\tilde{u_k}| \right), \tag{21}$$

where $\zeta_0 = \max_{0 \le k \le N} \{ |\tilde{u_0}| + \frac{\rho^{-\gamma} h^{\gamma} m_1 b_{k,0}}{\Gamma(\gamma+2)} |\tilde{u_0}| \}$. Here, C_{γ} is a positive constant dependent to γ (Lemma 1) and h is possibly small. From Lemma 2, we get $|\tilde{u}_{k+1}| \le \mathcal{C} \zeta_0$, where $\mathcal{C}$ is a positive constant independent to k and h. This gives the required result. □

3.2 Error analysis

Lemma 3 [43] *Let $u(t)$ be the solution of (12), and $x(t,u)$ be continuous and satisfies the Lipschitz condition with respect to u for a sufficiently small h. Then, we have*

$$\begin{aligned}
&\Big| \int_0^{t_{n+1}^{\rho}} s^{\rho-1} (t_{n+1}^{\rho} - s^{\rho})^{\gamma-1} x(s, u(t)) \mathrm{d}s \\
&\quad - \frac{\rho^{-\gamma} h^{\gamma}}{\gamma} \sum_{m=0}^{n} b_{m,n+1} x(t_m, u(t_m)) \Big| \le C_2 h^{\sigma(\gamma)}.
\end{aligned}$$

Theorem 5 *For the proposed scheme (16), we have*

$$|u(t_{k+1}) - u_{k+1}| \le C h^{\gamma}, \ k = 0, \ldots, N-1, \tag{22}$$

where C is a positive constant independent to h and k.

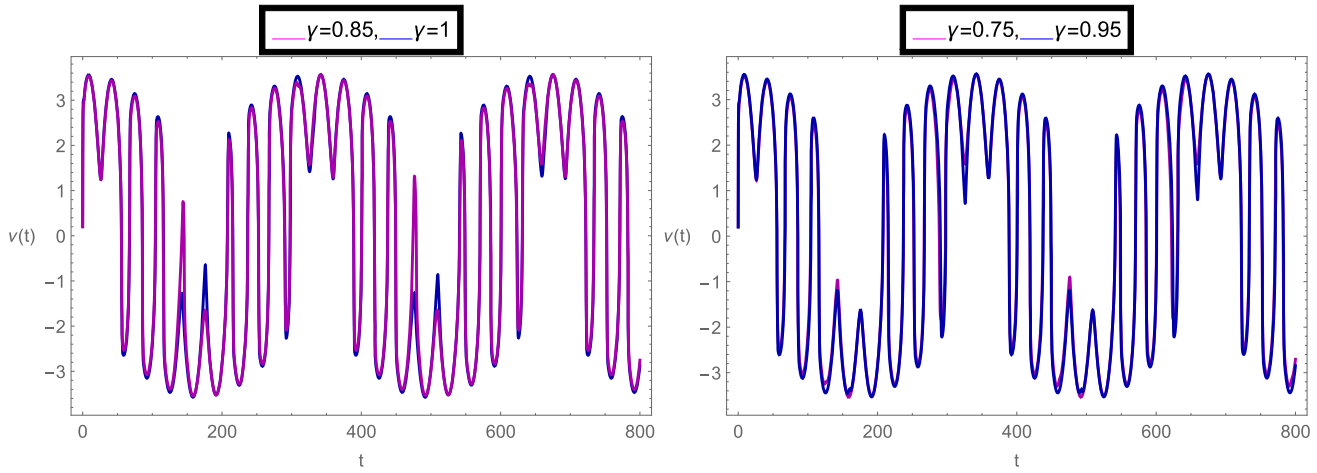

(a) voltage $v(t)$ (b) voltage $v(t)$

Fig. 5 Parameter values: $k_1 = 1.0$, $I_1 = 6.0$, $f_1 = 0.06$, $I_2 = 6.0$, $f_2 = 0.006$, $\lambda_H = 1.0$, $\alpha = 0.01$, $\beta = 0.02$, $k_2 = 1.0$, $\lambda_E = 1.0$, $a = 0.2$, $b = 0.1$, $k_3 = 1.0$, $k_4 = 0.01$

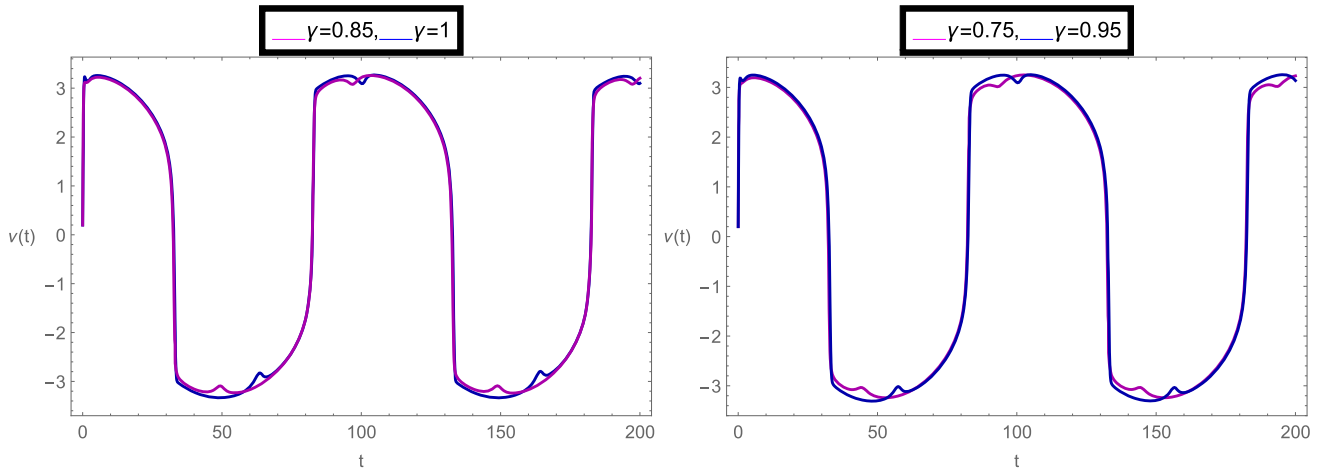

(a) voltage $v(t)$ (b) voltage $v(t)$

Fig. 6 At parameters: $k_1 = 1.0$, $I_1 = 0.0$, $f_1 = 0.0$, $I_2 = 6.0$, $f_2 = 0.02$, $\lambda_H = 1.0$, $\alpha = 1.0$, $\beta = 0.02$, $k_2 = 1.0$, $\lambda_E = 1.0$, $a = 0.2$, $b = 0.1$, $k_3 = 1.0$, $k_4 = 0.01$

Proof Let $u(t_0) = u_0$, and $e_k = u(t_k) - u_k$. Using the Volterra Eq. (6) and applying Eq. (16), we define the error expression as follows:

$$u(t_{k+1}) - u_{k+1} = \frac{\rho^{1-\gamma}}{\Gamma(\gamma)} \int_0^t s^{\rho-1}(t^\rho - s^\rho)^{\gamma-1} x(s,u)\mathrm{d}s - \frac{\rho^{-\gamma}h^\gamma}{\Gamma(\gamma+1)} \sum_{j=0}^{k} b_{j,k+1} x(t_j, u_j).$$

Therefore,

$$|u(t_{k+1}) - u_{k+1}| = |\frac{\rho^{1-\gamma}}{\Gamma(\gamma)} \int_0^t s^{\rho-1}(t^\rho - s^\rho)^{\gamma-1} x(s,u)\mathrm{d}s - \frac{\rho^{-\gamma}h^\gamma}{\Gamma(\gamma+1)} \sum_{j=0}^{k} b_{j,k+1} x(t_j, u_j)|$$

$$\leq |\frac{\rho^{1-\gamma}}{\Gamma(\gamma)} \int_0^t s^{\rho-1}(t^\rho - s^\rho)^{\gamma-1} x(s,u)\mathrm{d}s - \frac{\rho^{-\gamma}h^\gamma}{\Gamma(\gamma+1)} \sum_{j=0}^{k} b_{j,k+1} x(t_j, u(t_j)| + \frac{\rho^{-\gamma}h^\gamma}{\Gamma(\gamma+1)} \sum_{j=1}^{k} b_{j,k+1} |x(t_j, u_{(t_j)} - x(t_j, u_j)|$$

$$\leq \frac{\mathcal{C}_2}{\Gamma(\gamma)} h^{\sigma(\gamma)} + \frac{L\rho^{-\gamma}h^\gamma}{\Gamma(\gamma+1)} \sum_{j=1}^{k} b_{j,k+1} |e_j|$$

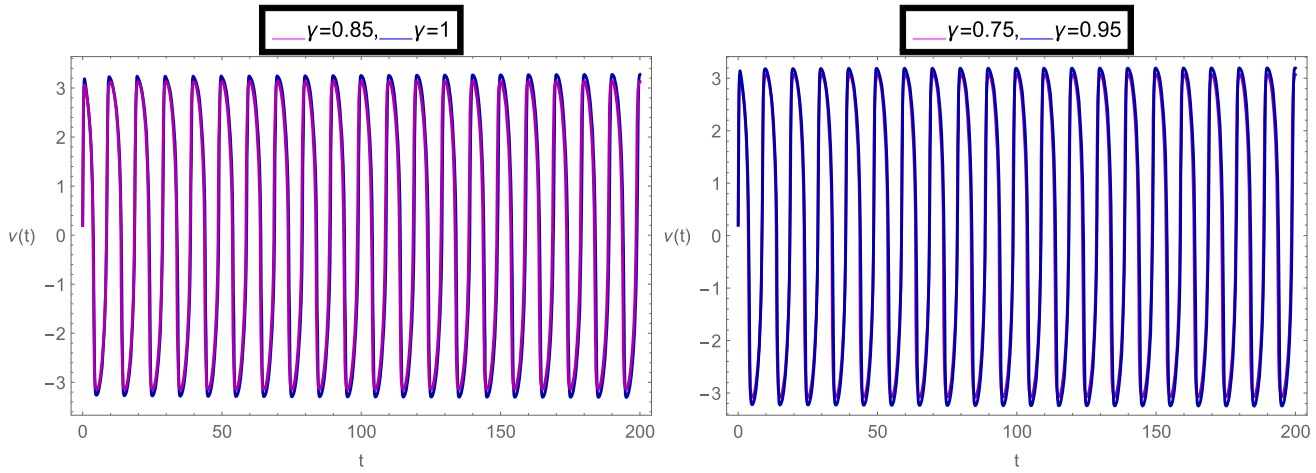

(a) voltage $v(t)$ (b) voltage $v(t)$

Fig. 7 At parameters: $k_1 = 1.0, I_1 = 0.0, f_1 = 0.0, I_2 = 6.0, f_2 = 0.2, \lambda_H = 1.0, \alpha = 1.0, \beta = 0.02, k_2 = 1.0, \lambda_E = 1.0, a = 0.2, b = 0.1, k_3 = 1.0, k_4 = 0.01$

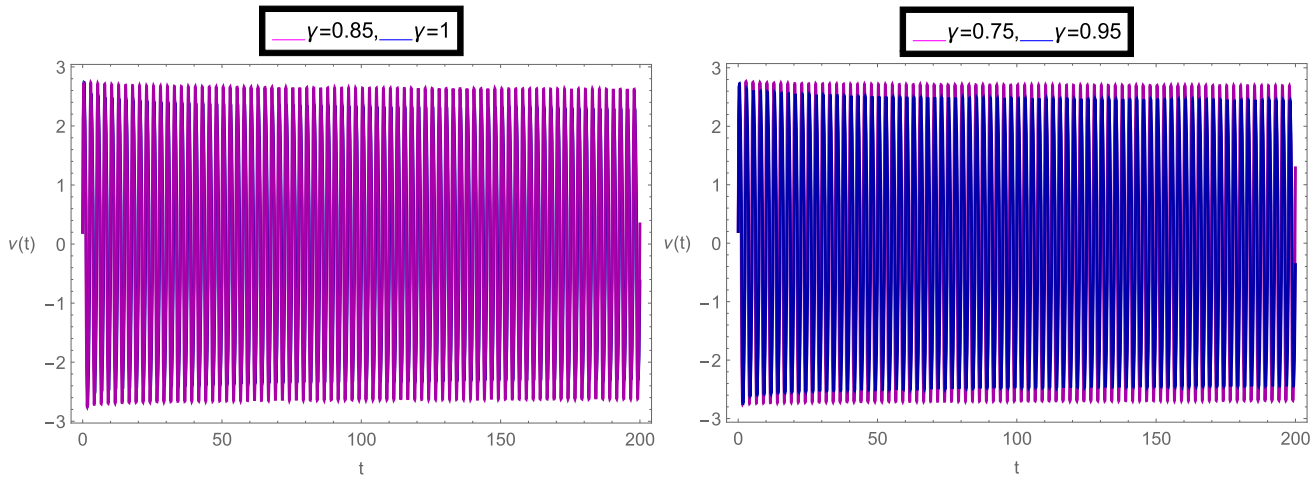

(a) voltage $v(t)$ (b) voltage $v(t)$

Fig. 8 At parameters: $k_1 = 1.0, I_1 = 0.0, f_1 = 0.0, I_2 = 6.0, f_2 = 0.8, \lambda_H = 1.0, \alpha = 1.0, \beta = 0.02, k_2 = 1.0, \lambda_E = 1.0, a = 0.2, b = 0.1, k_3 = 1.0, k_4 = 0.01$

$$\leq \frac{\mathcal{C}_2}{\Gamma(\gamma)} h^{\sigma(\gamma)} + \frac{L\mathcal{C}_{\gamma,1}\rho^{-\gamma}h^{\gamma}}{\Gamma(\gamma+1)} \sum_{j=1}^{k} (k+1-j)^{\gamma-1}|e_j|, \tag{23}$$

where we used Lemmas 3, 1, and the Lipschitz property. Using Lemma 2, we get the required results. □

4 Graphical simulations

Now we derive the numerical solution of the model (2) using the above-mentioned generalized Euler algorithm (18). The step size is fixed as $h = 0.01$ and extra parameter $\rho = 0.98$, which generates a non-uniform grid Eq. (11). The initial values are fixed as $(v_0, i_0, q_0, w_0) = (0.2, 0.01, 0.2, 0.01)$. We fix the parameters $k_1 = 1.0, k_2 = 1.0, k_3 = 1.0, k_4 = 0.01$.

For the parameter values $a = 0.2, b = 0.1, \alpha = 1.0, \beta = 0.02$, the charge- and magnetic flux-controlled memristor can represent nonlinear electrical bustling. In Fig. 1, the phase plots of membrane potential $v(t)$ versus current $i(t)$ are plotted for the given parameter values at fractional orders $\gamma = 0.85, 1$ (Fig. 1a) and $\gamma = 0.75, 0.95$ (Fig. 1b), respectively. Here, we notice that the phase portraits are nearly the same at each of the fractional-order values.

We know that the behavior of the plots is incumbent on the frequency of the external forcing current factor I_{ext} because

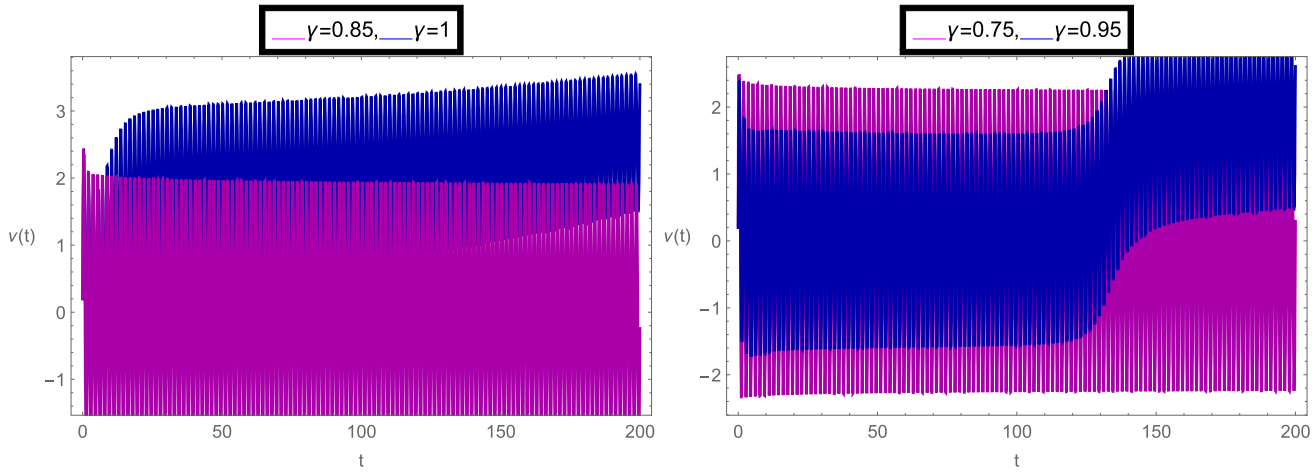

(a) voltage $v(t)$ (b) voltage $v(t)$

Fig. 9 At parameters: $k_1 = 1.0, I_1 = 0.0, f_1 = 0.0, I_2 = 6.0, f_2 = 1.2, \lambda_H = 1.0, \alpha = 1.0, \beta = 0.02, k_2 = 1.0, \lambda_E = 1.0, a = 0.2, b = 0.1, k_3 = 1.0, k_4 = 0.01$

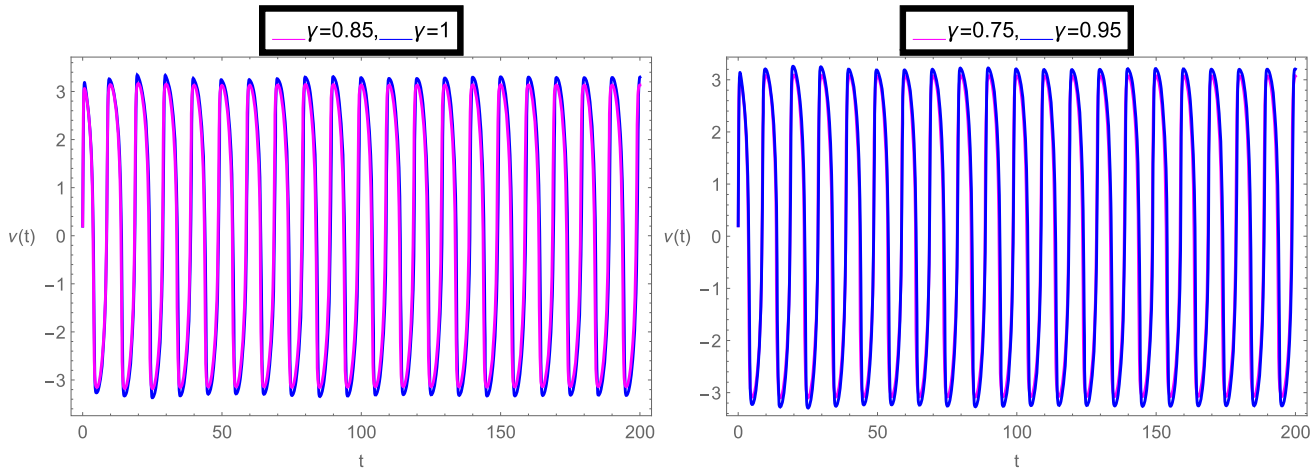

(a) voltage $v(t)$ (b) voltage $v(t)$

Fig. 10 At parameters: $k_1 = 1.0, I_1 = 0.0, f_1 = 0.0, I_2 = 6.0, f_2 = 0.2, \lambda_H = 1.0, \alpha = 1.0, \beta = 0.02, k_2 = 1.0, \lambda_E = 1.0, a = 0.2, b = 0.1, k_3 = 1.0, k_4 = 0.01, V_{th} = 1.0, A_0 = 0.01, A_1 = 0.1, B_1 = 0.1, A_2 = 0.1, B_2 = 0.1$

the exciting state can be disposed of by the external forcing. Therefore, to check the mode dependency of electrical bustling on external excitation, we plotted Fig. 2 by changing $f_2 = 0.06$ to $f_2 = 6.66$ (other parameter values are the same as for Fig. 1). Here, we see that the phase diagrams Fig. 2a, b differ from the plots of Fig. 1 which justifies that the multiple modes can be generated in the electrical bustling.

In the previous two cases, the electromagnetic field was not incorporated as $\lambda_E = \lambda_H = 0$. In Fig. 3, we consider the electromagnetic field changing with time taking $\lambda_E = 1.0, \lambda_H = 1.0$. Also, the electrical movements of an isolated neuron are explored with $I_1 = I_2 = 6.0, f_1 = 0.06, f_2 = 0.06$.

In Fig. 4, we take $f_2 = 6.66$ (other parameter values are same as for Fig. 3). Here, we see that Fig. 4a, b shows that the phase portraits become dense and periodic phases are converted into chaotic phases. In particular, we can see that the phase portraits obtained at fractional orders $\gamma = 0.85, 0.75$ are denser compared to the nearest values of $\gamma = 1$. This justifies that fractional-order cases generate more varieties in the phase portraits between $v(t)$ and $i(t)$.

In Fig. 5, the firing patterns of neural activities are plotted for the parameter values $k_1 = 1.0, I_1 = 6.0, f_1 = 0.06, I_2 = 6.0, f_2 = 0.006, \lambda_H = 1.0, \alpha = 0.01, \beta = 0.02, k_2 = 1.0, \lambda_E = 1.0, a = 0.2, b = 0.1, k_3 = 1.0, k_4 = 0.01$ at the given fractional-order values. Here, we notice

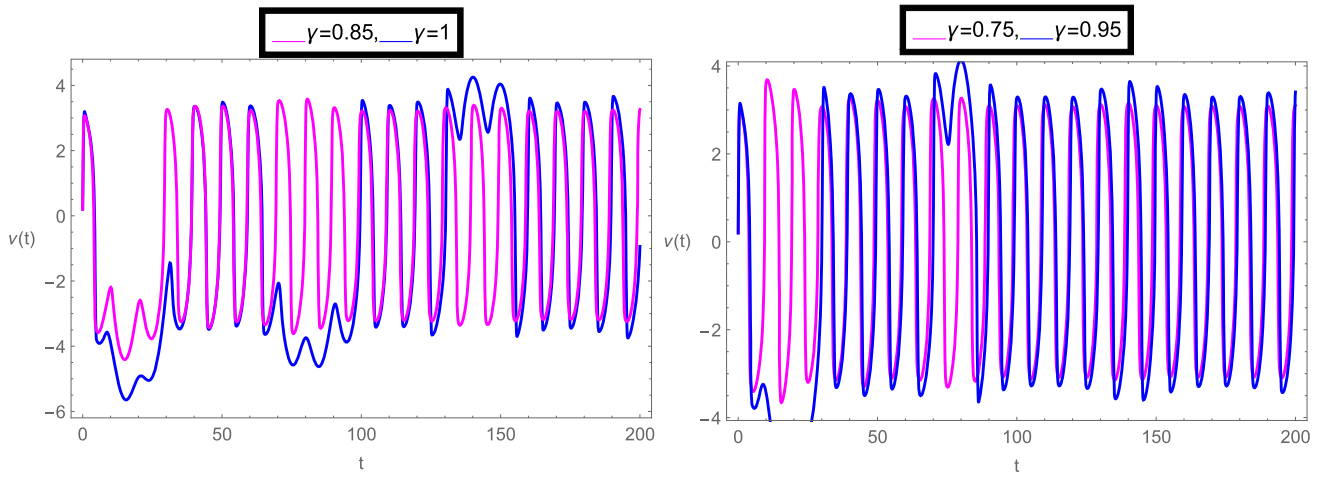

(a) voltage $v(t)$ (b) voltage $v(t)$

Fig. 11 At parameters: $k_1 = 1.0, I_1 = 0.0, f_1 = 0.0, I_2 = 6.0, f_2 = 0.2, \lambda_H = 1.0, \alpha = 1.0, \beta = 0.02, k_2 = 1.0, \lambda_E = 1.0, a = 0.2, b = 0.1, k_3 = 1.0, k_4 = 0.01, V_{th} = 1.0, A_0 = 0.01, A_1 = 1.1, B_1 = 0.1, A_2 = 0.1, B_2 = 0.1$

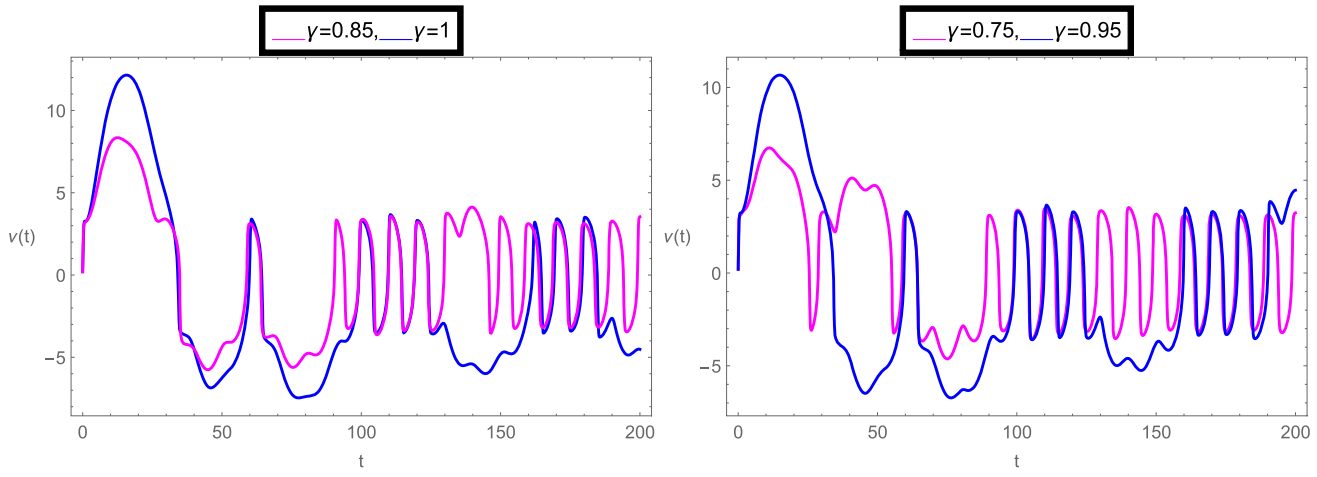

(a) voltage $v(t)$ (b) voltage $v(t)$

Fig. 12 At parameters: $k_1 = 1.0, I_1 = 0.0, f_1 = 0.0, I_2 = 6.0, f_2 = 0.2, \lambda_H = 1.0, \alpha = 1.0, \beta = 0.02, k_2 = 1.0, \lambda_E = 1.0, a = 0.2, b = 0.1, k_3 = 1.0, k_4 = 0.01, V_{th} = 1.0, A_0 = 0.01, A_1 = 3.1, B_1 = 0.1, A_2 = 0.1, B_2 = 0.1$

that in each fractional-order case, the dynamics of the plots is same.

Using the external forcing current, we can adjust the excitability which results in the various firing patterns. Now we consider the various value of I_{ext} by changing the values of frequency f_2, whereas the frequency f_1 is fixed at zero. From the group of Figs. 6, 7, 8, and 9, we can see that the electrical movements can be controlled to produce periodic oscillations when I_{ext} is incorporated with various frequencies. From Fig. 9, we notice that at fractional order values $\gamma = 0.75, 0.85$, the patterns of membrane potential are more uniform compared to the nearest values of fractional order $\gamma = 1$.

As experimented in ref. [33], the magnetic excitation was incorporated by a circular induction coil on the neural circuit when external electromagnetic radiation was imposed. In this case, the new revised model is given as follows:

$$\begin{aligned}
{}_0^C D_t^{\gamma,\rho} v &= -\left(\frac{v^3}{3} - k_1 v\right) - i \\
&\quad + I_{ext} + \lambda_H(\alpha + 3\beta w^2)v, \\
{}_0^C D_t^{\gamma,\rho} i &= v - k_2 i - \lambda_E(a + bq^2)i, \\
{}_0^C D_t^{\gamma,\rho} q &= k_3 i, \\
{}_0^C D_t^{\gamma,\rho} w &= -k_4 v + V_{th} \exp(-A_0 t)[A_1 \cos(B_1 t) \\
&\quad + A_2 \sin(B_2 t)],
\end{aligned} \tag{24}$$

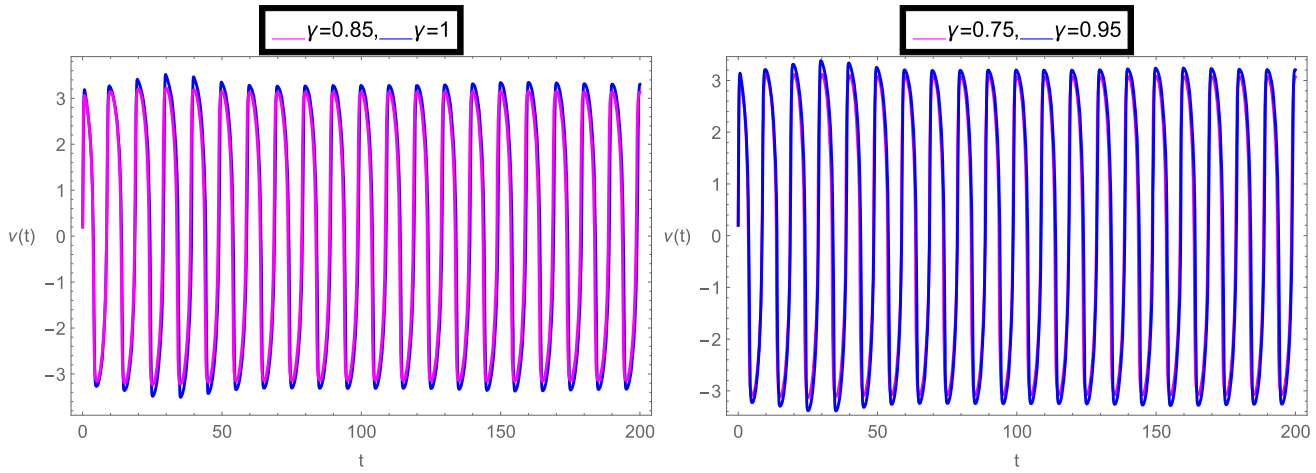

(a) voltage $v(t)$ (b) voltage $v(t)$

Fig. 13 At parameters: $k_1 = 1.0, I_1 = 0.0, f_1 = 0.0, I_2 = 6.0, f_2 = 0.2, \lambda_H = 1.0, \alpha = 1.0, \beta = 0.02, k_2 = 1.0, \lambda_E = 1.0, a = 0.2, b = 0.1, k_3 = 1.0, k_4 = 0.01, V_{th} = 1.0, A_0 = 0.01, A_1 = 0.1, B_1 = 0.05, A_2 = 0.1, B_2 = 0.1$

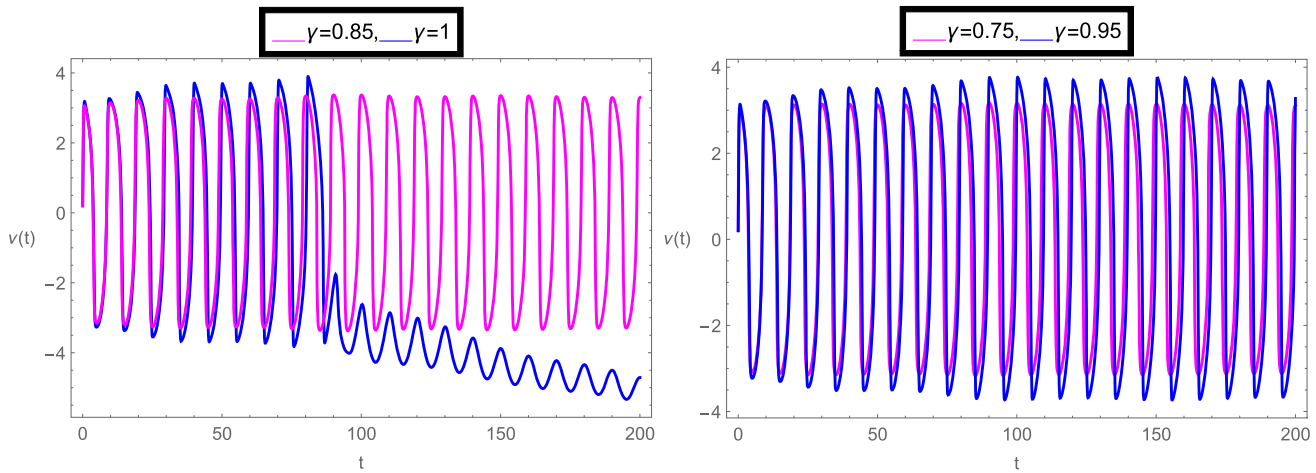

(a) voltage $v(t)$ (b) voltage $v(t)$

Fig. 14 At parameters: $k_1 = 1.0, I_1 = 0.0, f_1 = 0.0, I_2 = 6.0, f_2 = 0.2, \lambda_H = 1.0, \alpha = 1.0, \beta = 0.02, k_2 = 1.0, \lambda_E = 1.0, a = 0.2, b = 0.1, k_3 = 1.0, k_4 = 0.01, V_{th} = 1.0, A_0 = 0.01, A_1 = 0.1, B_1 = 0.01, A_2 = 0.1, B_2 = 0.1$

where the term $V_{th} \exp(-A_0 t)[A_1 \cos(B_1 t) + A_2 \sin(B_2 t)]$ defines the external electromagnetic radiation incorporated by a stimulator coil and V_{th} is the induction potential threshold. A_0, A_1, A_2, and B_1, B_2 are the damping ratio, amplitudes, and angular frequencies of source of radiation, simultaneously. The meaning of occurrence of large diversity in B_1, B_2 is the both low- and high-frequency signals are interpolated on the neuron, respectively.

Now we plot the numerical solution of this new revised model (24) using the aforementioned generalized Euler algorithm (18). In the cluster of Figs. 10, 11, 12, 13, 14, and 15, we plotted the time-series graphs of membrane potential in an isolate neuron changing the amplitude A_1 or frequency B_1 in the external magnetic radiation when $V_{th} = 1.0$, $A_0 = 0.01$.

In Figs. 10, 11, and 12, the frequency B_1 is fixed at $B_1 = 0.1$ where the amplitude A_1 is taken as $A_1 = 0.1$ (Fig. 10a, b), $A_1 = 1.1$ (Fig. 11a, b), $A_1 = 3.1$ (Fig. 12a, b). It is noticed in Fig. 11 that near to the fractional order $\gamma = 1, 0.95, 0.85$, the periodic solutions are disturbed but at fractional order $\gamma = 0.75$, the periodic solutions nearly to be exists. This justifies the possibility of the existence of various solutions in the case of fractional derivatives.

In Figs. 13, 14, and 15, the amplitude A_1 is fixed at $A_1 = 0.1$ where the frequency B_1 is taken as $B_1 = 0.05$ (Fig. 13a, b), $B_1 = 0.01$ (Fig. 14a, b), $B_1 = 0.001$ (Fig. 15a, b). It is noticed in Figs. 14 and 15 that near to the fractional order $\gamma = 1, 0.95$, the solutions are not perfectly periodic but at fractional order $\gamma = 0.85, 0.75$, the periodic solution exists.

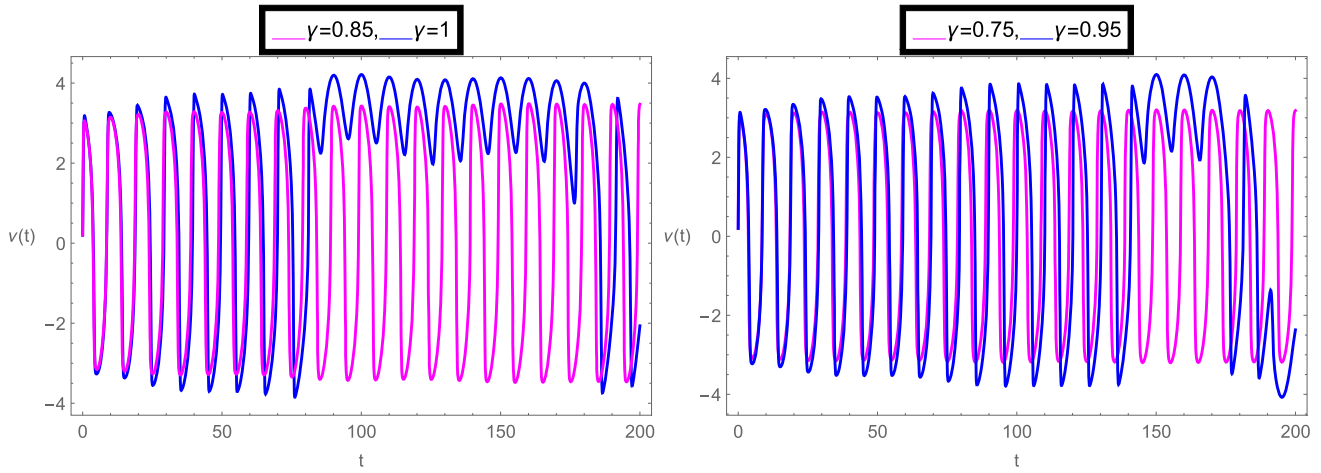

(a) voltage $v(t)$ (b) voltage $v(t)$

Fig. 15 At parameters: $k_1 = 1.0, I_1 = 0.0, f_1 = 0.0, I_2 = 6.0, f_2 = 0.2, \lambda_H = 1.0, \alpha = 1.0, \beta = 0.02, k_2 = 1.0, \lambda_E = 1.0, a = 0.2, b = 0.1, k_3 = 1.0, k_4 = 0.01, V_{th} = 1.0, A_0 = 0.01, A_1 = 0.1, B_1 = 0.001, A_2 = 0.1, B_2 = 0.1$

From the graphical observations, we notice that fractional orders may change the behavior of the solution because of memory effects. The simulations are performed in *Mathematica*. The suggested methodology is not just restricted to simulating the proposed types of neuron models. This scheme can be used in modern control systems such as optimal deep learning control for modernized microgrids [45], fuzzy control for current sharing and voltage balancing in microgrids [46], etc.

5 Conclusions

In this study, we have investigated the dynamics of a fractional-order neuron model using generalized Caputo fractional derivatives. We have given proof of the existence of a unique solution for the proposed model. A new version of the Euler method has been used to derive the numerical solution of the model. The stability and error estimation have been proved for the proposed numerical scheme. In the graphical simulations, the influences of model parameters have been explored, and the results are explained briefly. From the performed analysis, we conclude that the fractional-order values provide more degree of freedom in the solutions and justify most of the possible cases of the proposed neuron model outputs. In the future, the given neuron model can be redefined using any other fractional derivative, or the same model can be revisited after a new circuit experiment. Moreover, some theoretical simulations of the stability and bifurcation of the system can be performed.

Author Contributions All authors equally contributed to this work.

Funding Open access funding provided by University of Johannesburg. NA.

Data availability The data used in this research are available/mentioned within the manuscript.

Declarations

Conflict of interest This work does not have any conflicts of interest.

Code availability Not applicable.

References

1. Hodgkin AL, Huxley AF (1952) A quantitative description of membrane current and its application to conduction and excitation in nerve. J Physiol 117(4):500
2. Stein RB (1965) A theoretical analysis of neuronal variability. Biophys J 5(2):173–194
3. Monroe D (2014) Neuromorphic computing gets ready for the (really) big time, 57(6):13–15
4. Ochs K, Michaelis D, Jenderny S (2018) An optimized morris-lecar neuron model using wave digital principles. In 2018 IEEE 61st

international midwest symposium on circuits and systems (MWSCAS), IEEE, pp 61–64
5. Usha K, Subha PA (2019) Hindmarsh-Rose neuron model with memristors. Biosystems 178:1–9
6. Grill-Spector K, Henson R, Martin A (2006) Repetition and the brain: neural models of stimulus-specific effects. Trends Cogn Sci 10(1):14–23
7. Gu H, Pan B (2015) A four-dimensional neuronal model to describe the complex nonlinear dynamics observed in the firing patterns of a sciatic nerve chronic constriction injury model. Nonlinear Dyn 81(4):2107–2126
8. Wang C, Ma J (2018) A review and guidance for pattern selection in spatiotemporal system. Int J Mod Phys B 32(06):1830003
9. Kilbas A, Srivastava HM, Trujillo JJ (2006) Theory and applications of fractional differential equations. Elsevier Science
10. Podlubny I (1998) Fractional differential equations: an introduction to fractional derivatives, fractional differential equations, to methods of their solution and some of their applications. Elsevier
11. Oldham K, Spanier J (1974) The fractional calculus theory and applications of differentiation and integration to arbitrary order. Elsevier
12. Caputo M, Fabrizio M (2015) A new definition of fractional derivative without singular kernel. Progr Fract Differ Appl 1(2):1–13
13. Kumar P, Suat Erturk V, Nisar KS (2021) Fractional dynamics of huanglongbing transmission within a citrus tree. Math Methods Appl Sci 44(14):11404–11424
14. Kumar P, Govindaraj V, Erturk VS, Abdellattif MH (2022) A study on the dynamics of alkali-silica chemical reaction by using Caputo fractional derivative. Pramana 96(3):1–19
15. Erturk VS, Ahmadkhanlu A, Kumar P, Govindaraj V (2022) Some novel mathematical analysis on a corneal shape model by using Caputo fractional derivative. Optik 261:169086
16. Vellappandi M, Kumar P, Govindaraj V (2022) Role of vaccination, the release of competitor snails, chlorination of water, and treatment controls on the transmission of bovine schistosomiasis disease: a mathematical study. Phys Script 97(7):074006
17. Etemad S, Avci I, Kumar P, Baleanu D, Rezapour S (2022) Some novel mathematical analysis on the fractal–fractional model of the AH1N1/09 virus and its generalized Caputo-type version. Chaos, Solit Fract 162:112511
18. Baleanu D, Sajjadi SS, Asad JH, Jajarmi A, Estiri E (2021) Hyperchaotic behaviors, optimal control, and synchronization of a nonautonomous cardiac conduction system. Adv Diff Equ 2021(1):1–24
19. Baleanu D, Sajjadi SS, Jajarmi AMIN, Defterli OZLEM, Asad JH, Tulkarm P (2021) The fractional dynamics of a linear triatomic molecule. Rom Rep Phys 73(1):105
20. Moaddy K, Radwan AG, Salama KN, Momani S, Hashim I (2012) The fractional-order modeling and synchronization of electrically coupled neuron systems. Comput Math Appl 64(10):3329–3339
21. Teka W, Marinov TM, Santamaria F (2014) Neuronal spike timing adaptation described with a fractional leaky integrate-and-fire model. PLoS Comput Biol 10(3):e1003526
22. Armanyos M, Radwan AG (2016) Fractional-order Fitzhugh–Nagumo and Izhikevich neuron models. In 2016 13th international conference on electrical engineering/electronics, computer, telecommunications and information technology (ECTI-CON), IEEE, pp 1–5
23. Teka WW, Upadhyay RK, Mondal A (2018) Spiking and bursting patterns of fractional-order Izhikevich model. Commun Nonlinear Sci Numer Simul 56:161–176
24. Khanday FA, Kant NA, Dar MR, Zulkifli TZA, Psychalinos C (2018) Low-voltage low-power integrable CMOS circuit implementation of integer-and fractional-order FitzHugh–Nagumo neuron model. IEEE Trans Neural Netw Learn Syst 30(7):2108–2122
25. Rajagopal K, Nazarimehr F, Karthikeyan A, Alsaedi A, Hayat T, Pham VT (2019) Dynamics of a neuron exposed to integer-and fractional-order discontinuous external magnetic flux. Front Inf Technol Electron Eng 20(4):584–590
26. Tolba MF, Elsafty AH, Armanyos M, Said LA, Madian AH, Radwan AG (2019) Synchronization and FPGA realization of fractional-order Izhikevich neuron model. Microelectron J 89:56–69
27. Malik SA, Mir AH (2020) Synchronization of fractional order neurons in presence of noise. IEEE/ACM Trans Comput Biol Bioinform 19(3):1887–1896
28. Malik SA, Mir AH (2020) FPGA realization of fractional order neuron. Appl Math Model 81:372–385
29. Ramadoss J, Aghababaei S, Parastesh F, Rajagopal K, Jafari S, Hussain I (2021) Chimera state in the network of fractional-order fitzhugh-nagumo neurons. Complexity. https://doi.org/10.1155/2021/2437737
30. Dar MR, Kant NA, Khanday FA (2022) Dynamics and implementation techniques of fractional-order neuron models: a survey. In: Fractional order systems, Academic Press, pp 483-511
31. AbdelAty AM, Fouda ME, Eltawil AM (2022) On numerical approximations of fractional-order spiking neuron models. Commun Nonlinear Sci Numer Simul 105:106078
32. Dar MR, Kant NA, Khanday FA, Malik SA, Kharadi MA (2022) Analog and digital implementation of fractional-order FitzHugh–Nagumo (FO-FHN) neuron model. In: Fractional-Order modeling of dynamic systems with applications in optimization, signal processing and control, Academic Press, pp 475–504
33. Wu F, Ma J, Zhang G (2019) A new neuron model under electromagnetic field. Appl Math Comput 347:590–599
34. Odibat Z, Baleanu D (2020) Numerical simulation of initial value problems with generalized caputo-type fractional derivatives. Appl Numer Math 156:94–105
35. Erturk VS, Kumar P (2020) Solution of a COVID-19 model via new generalized Caputo-type fractional derivatives. Chaos Solit Fract 139:110280
36. Jhinga A, Daftardar-Gejji V (2018) A new finite-difference predictor–corrector method for fractional differential equations. Appl Math Comput 336:418–432
37. Kumar P, Erturk VS, Kumar A (2021) A new technique to solve generalized Caputo type fractional differential equations with the example of computer virus model. J Math Ext 15
38. Odibat Z, Erturk VS, Kumar P, Govindaraj V (2021) Dynamics of generalized Caputo type delay fractional differential equations using a modified Predictor–Corrector scheme. Phys Script 96(12):125213
39. Odibat Z, Erturk VS, Kumar P, Ben Makhlouf A, Govindaraj V (2022) An implementation of the generalized differential transform scheme for simulating impulsive fractional differential equations. Math Probl Eng
40. Abd-Elhameed WM, Youssri Y (2017) Generalized Lucas polynomial sequence approach for fractional differential equations. Nonlinear Dyn 89(2):1341–1355
41. Shloof AM, Senu N, Ahmadian A, Salahshour S (2021) An efficient operation matrix method for solving fractal–fractional differential equations with generalized Caputo-type fractional-fractal derivative. Math Comput Simul 188:415–435
42. Youssri YH (2021) Orthonormal ultraspherical operational matrix algorithm for fractal–fractional Riccati equation with generalized Caputo derivative. Fract Fract 5(3):100
43. Kumar P, Erturk VS, Murillo-Arcila M, Harley C (2022) Generalized forms of fractional Euler and Runge-Kutta methods using non-uniform grid. Int J Nonlinear Sci Numer Simul. https://doi.org/10.1515/ijnsns-2021-0278/html

44. Li C, Zeng F (2013) The finite difference methods for fractional ordinary differential equations. Numer Funct Anal Opt 34(2):149–179
45. Yan SR, Guo W, Mohammadzadeh A, Rathinasamy S (2022) Optimal deep learning control for modernized microgrids. Appl Intell. https://doi.org/10.1007/s10489-022-04298-2
46. Taghieh A, Mohammadzadeh A, Zhang C, Kausar N, Castillo O (2022) A type-3 fuzzy control for current sharing and voltage balancing in microgrids. ApplSoft Comput 129:109636